Distribution and enrichment mechanism of helium in the Hetianhe gas field, Tarim Basin, northwest China

Jiahao Lv [a, b], Quanyou Liu [c, *], PengPeng Li [c], Jiarun Liu [c], Zheng Zhou [d]

[a] State Key Laboratory of Deep Petroleum Intelligent Exploration and Development, Institute of Geology and Geophysics, Chinese Academy of Sciences, Beijing, 100029, China

[b] College of Earth and Planetary Sciences, University of Chinese Academy of Sciences, Beijing, 101408, China

[c] Institute of Energy, Peking University, Beijing 100871, China

[d] Lancaster Environment Centre, Lancaster University, Lancaster, LA14YQ, UK

* The corresponding author.

E-mail address: liuqy@pku.edu.cn (Q. Liu)

ABSTRACT

Helium (He), as an irreplaceable and scarce strategic resource, is primarily extracted from natural gas for industrial and economic production. Constraining the distribution and enrichment mechanism of He in natural gas is crucial for the effectiveness of helium resource exploration and development. We report natural gas and noble gas isotopic composition in samples from three production areas in the Hetianhe He-rich gas field, Tarim Basin, northwest China. This study investigates differential enrichment of He in the Hetianhe gas field. The He content in the Hetianhe gas field ranges between 0.27% and 0.42%, with an average value of 0.33%. The He content increases gradually from east to west within the gas field and tends to accumulate in structurally high positions. $^3He/^4He$ ratios range from 0.045 to 0.076 Ra (where Ra is atmospheric ratio of $^3He/^4He$), with an average of 0.057 Ra, indicating that the helium is typically of crustal origin. The differential enrichment of helium in the Hetianhe gas field is primarily controlled by temperature and pressure conditions, lateral migration, and preservation conditions. Changes in temperature and pressure, especially differences caused by tectonic uplift, lead to degassing, resulting in relative enrichment of helium in structurally high positions. A gas solubility model was used to quantify the subsurface fluid migration pathways and it suggests that, from the eastern production area to the middle production area and then to the western production area, the natural gas/groundwater volume ratio (V_g/V_w) gradually decreases, corresponding to 1.40, 0.35, 0.16, respectively. The V_g/V_w ratio

indicates that helium-rich natural gas has undergone lateral migration from east to west. As the migration distance increases, the content of radiogenic isotopes (e.g., ^{4}He and ^{40}Ar) gradually increases. This suggests that during the migration, the helium-rich natural gas continuously extracts radiogenic isotopes, leading to the differential enrichment of helium. It is noteworthy that, compared to degassing, the extraction process may be the primary enrichment mechanism for helium in the Hetianhe gas field. Additionally, the distribution of east-west gypsum-mudstone cap layers results in differential vertical diffusion of helium, which macroscopically controls the differential enrichment of helium. The migration and accumulation of helium exhibit a certain synergy with hydrocarbon reservoir formation. Ultimately, a five-stage conceptual model has been developed in this study to explain the differential enrichment of helium in the Hetianhe gas field.

Keywords: Helium; Natural gas; Enrichment mechanism; Lateral migration; Hetianhe gas field

1 Introduction

Due to its unique physical and chemical properties, helium is widely used in high-tech fields and is an irreplaceable, critical strategic resource essential for national security and the development of high-tech industries (Ballentine and Burnard, 2002; Dai et al., 2017; Danabalan et al., 2022). In addition, helium, as a global resource, faces issues of supply-demand imbalance and scarcity due to various countries enacting helium resource protection laws and fluctuations in the global helium market (Siddhantakar et al., 2023; Liu et al., 2023). Extracting helium from natural gas remains the primary method for industrial helium production globally (Wang et al., 2023; Cheng et al., 2023). Therefore, identifying helium-rich natural gas with industrial extraction potential becomes the most direct approach to addressing global helium resource shortages.

Helium primarily originates from three sources: atmospheric, crustal, and mantle. In petroliferous basins, crustal helium (^{4}He) is predominant. Crustal helium is produced from the radioactive decay of uranium (U) and thorium (Th) in minerals and rocks. The radioactive decay reactions are: ^{238}U→8^{4}He+6β+^{206}Pb, ^{235}U→7^{4}He+4β+^{207}Pb, ^{232}Th→6^{4}He+4β+^{208}Pb (Ballentine and Burnard, 2002; Danabalan et al., 2022). Helium is released from mineral lattices, intergranular spaces, or inclusions through diffusion, recoil, fracturing, and mineral conversion processes, and then enters pores or dissolves in pore water. Subsequently, it migrates and accumulates in favorable traps (Ballentine and Burnard, 2002; Brown, 2010). Previous studies on the enrichment and accumulation processes of helium are relatively limited and predominantly qualitative in nature. Ballentine and Burnard (2002) suggest that helium content in the crust is low and helium cannot diffuse independently. Helium must rely on fluids in rock pores for vertical migration and accumulation along basement faults. Brown (2010) divides the process of helium enrichment and accumulation into primary migration and secondary migration phases. Helium generated from

64 element decay in sedimentary layers diffuses into formation water, and helium-bearing formation
65 water accumulates under appropriate shallow conditions for reservoir formation. Ballentine et al.
66 (2002) and Brown (2010) both argue that the helium in the giant Panhandle helium field in the
67 United States enriches and accumulates after migration and precipitation through groundwater.
68 Cheng et al. (2023), combining sedimentary basin evolution, established a gas diffusion model
69 revealing the coupled enrichment mechanism of He and N_2. Feng et al. (2024) discussed the
70 mechanisms of helium migration and accumulation under deep thermal fluid activity in the Yingge
71 Basin, indicating primary migration of helium by convection, controlled by the mixing of crust-
72 mantle gases and processes such as hydrothermal degassing and gas-liquid separation from deep to
73 shallow layers. Wang et al. (2023) studied the enrichment process of mantle-derived helium in oil
74 and gas basins in eastern China, suggesting that the enrichment of mantle-derived He is mainly
75 related to CO_2 dissolution and mineralization.

76   Noble gas isotopic compositions serve as ideal tracers for studying interactions among
77 subsurface fluids (Ballentine and Burnard, 2002; Zhou et al., 2005). Due to their chemical inertness,
78 their abundance in geological fluids is controlled by physical processes such as dissolution,
79 adsorption, and diffusion. The characteristics of noble gases in the Earth's major reservoirs (crust,
80 mantle, and atmosphere) are well-defined. Based on changes in rare gas isotopes, some scholars
81 have reconstructed the accumulation processes of helium (Barry et al., 2016; Barry et al., 2017;
82 Zhang et al., 2019a; Chen et al., 2019). Zhang et al. (2019b) used noble gas tracing techniques to
83 reconstruct the accumulation process of helium in the northern Qaidam Basin, revealing the
84 respective control of groundwater and hydrocarbons on the accumulation of helium in the
85 subsurface environment. Mtili et al. (2021) revealed that the accumulation of helium in Tanzania is
86 controlled by fault structures, interactions with groundwater, and proximity to magmatic
87 hydrothermal fluids, with varying degrees of mixture between crustal and mantle helium
88 contributing to present enrichment characteristics. Intense late-stage tectonic movements
89 significantly affect helium accumulation; when reservoirs undergo severe tectonic disturbances, the
90 loss of helium is much greater than that of hydrocarbon gases (Chen et al., 2019). Recent studies
91 have primarily focused on reconstructing migration carriers and accumulation processes (Zhang et
92 al., 2019a; Zhang et al., 2019b; Byrne et al., 2020; Halford et al., 2022), with fewer studies
93 specifically dedicated to investigating helium enrichment mechanisms.

94   Hetianhe gas field is the largest Paleozoic marine carbonate gas field discovered in the Tarim
95 Basin and also the first super-giant helium-rich gas field found in China (Tao et al., 2019). It
96 represents a crucial area for helium resource exploration in China. The Hetianhe gas field has a
97 stable geological structural background. However, a systematic study of the spatial distribution and
98 enrichment mechanisms of helium in this typical crustal-source gas field has not yet been conducted

99   from a resource perspective. This paper aims to elucidate the controlling mechanisms of differential

100   helium enrichment in typical crustal-source helium-rich natural gas fields, and establish a model for

101   helium enrichment. The goal is to provide new insights for the development and utilization of similar

102   helium-rich natural gas fields and further deepen the theoretical understanding of helium enrichment

103   and accumulation in such fields.

2 Geological setting

105   The Tarim Basin is a large composite basin developed beneath the Precambrian craton (Chen

106   et al., 2000; Du et al., 2018; Lai et al., 2021; Guo et al., 2022), comprising multiple tectonic units

107   (Fig. 1a). The study area, Hetianhe gas field, is located on the southern margin of the central uplift

108   of the Bachu uplift along the Mazatag structural belt (Fig. 1b), with a structural area of

109   approximately 450 km^2 (Zhu et al., 2019). The Hetianhe gas field contains two sets of hydrocarbon

110   source rocks from the Carboniferous-Permian and Cambrian periods, with the former being

111   transitional marine-terrestrial source rocks and the latter being marine source rocks (Song et al.,

112   2015). Studies indicate that the natural gas in the Hetianhe field primarily originates from the

113   Cambrian high-maturity marine source rocks (Liu et al., 2009; Zhu et al., 2019; Tao et al., 2019),

114   with the main reservoirs being Carboniferous clastic limestone and Ordovician buried hill carbonate

115   reservoirs. Additionally, in the Carboniferous, three sets of regional cap rocks are developed: the

116   upper shale section, middle shale section, and lower shale section. Moreover, zonal shale cap rocks

117   are developed above each sand layer in the Carboniferous sand-shale section (Wang et al., 2000;

118   Cai et al., 2002; Wu et al., 2011) (Fig. 1c).

119   The Hetianhe gas field is located on the Mazatag fault zone, which is a fault barrier tectonic

120   belt formed under the squeezing action of the Himalayan Age and sandwiched by two NW-SE

121   trending reverse faults. Three fault anticline structures Ma 8, Ma 2 and Ma 4 are developed from

122   west to east, respectively in the west, middle and east sections of the Mazatag structural zone (Fig.

123   2). Overall, it exhibits a west-high and east-low trend, with the axis of the structural belt generally

124   aligned with the direction of the faults (Cai et al., 2002; Ren et al., 2021). In the late Caledonian

125   period, the two northern and southern thrusting faults of the Hetianhe gas field were uplifted, and

126   the western part of the Hetianhe gas field was significantly more thrusting than the eastern part,

127   resulting in east-west differential uplift (Cai et al., 2002). With the continuous uplift of the Bachu

128   uplift at the end of the Indosinian period and the uplifting of the Kunlun mountain system in the

129   Himalayan period, the western uplift was subjected to intense denudation and formed the present

130   tectonic pattern of Hetianhe gas field, which is high in the west and low in the east. In addition,

131   there are significant differences in the geochemical characteristics of natural gas between the eastern

132   and western production area of the Hetianhe gas field. Previous studies have primarily attributed

these differences to two mechanisms: "dissolved gas" and "TSR reactions" (Qin et al., 2006; Zhu et al., 2019).
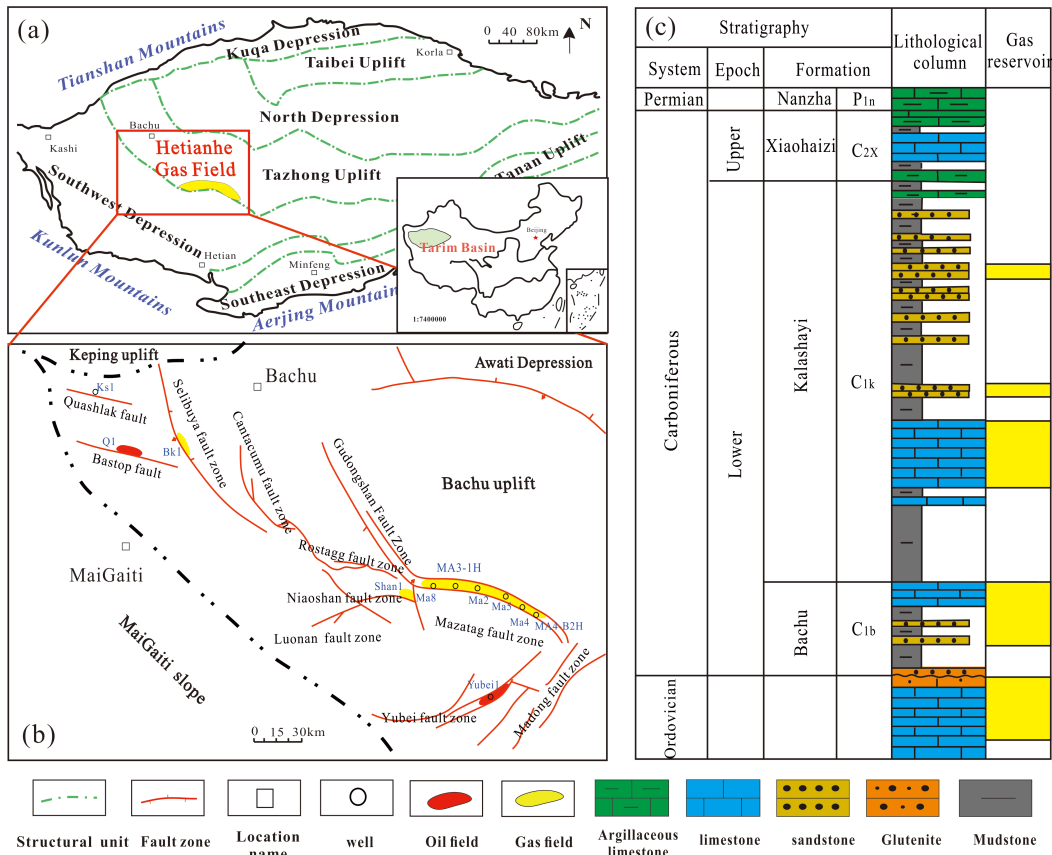
Fig. 1. (a) Main structural units of Tarim Basin; (b) Structural location of Hetianhe gas field; (c) Stratigraphic column of the Hetianhe gas Field (modified from Zhu et al. 2019)
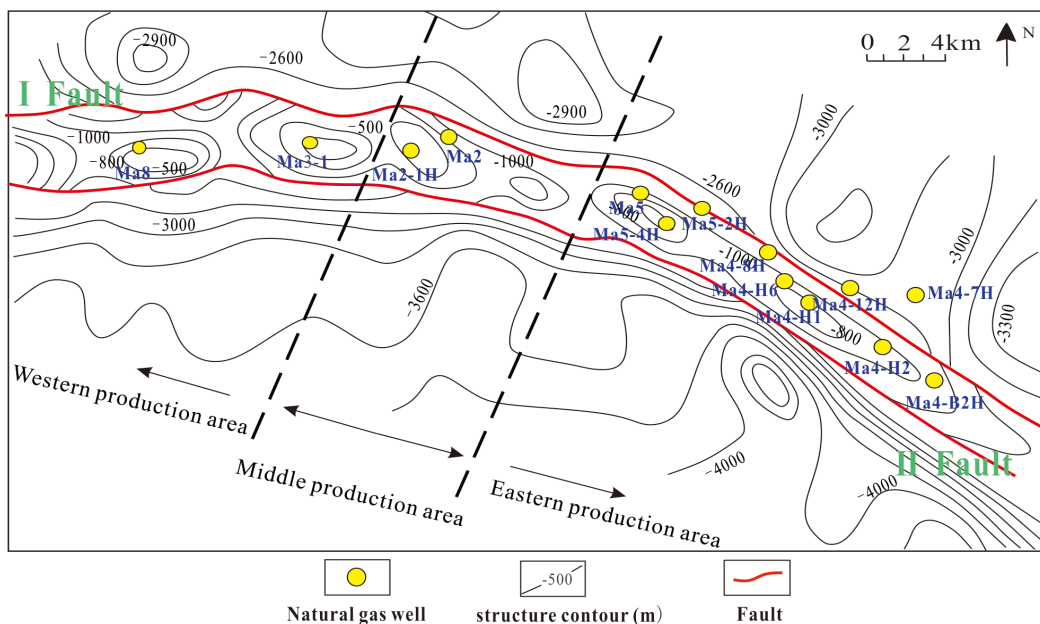
Fig. 2. Tectonic of the top surface of the Carboniferous biological limestone in the Hetanhe gas field (modified from Tao et al., 2019).

3 Samples and analytical methods

3.1 Samples

This study collected gas samples from 14 wells in the Hetianhe gas field. During sample collection, stainless steel cylinders with a diameter of 10 cm and a volume of approximately 1000 cm^3 were used, equipped with two stop valves with a maximum pressure of 22.5 MPa. During sampling, the pressure gauge at each wellhead was removed, and the cylinder was connected to the production pipeline. To eliminate air contamination, the pipeline was flushed for 10 minutes, and then the far-end and near-end valves of the cylinder were closed sequentially and repeated three times to ensure no air remained in the cylinder. After sample collection, the cylinder was immersed in water for leakage testing.

3.2 Analytical methods

The analyses of major natural gas components, as well as the concentrations and isotopes of noble gases, were analyzed in the Oil and Gas Research Center, Northwest Institute of Eco-Environment and Resources, Chinese Academy of Sciences. The major gas components were analyzed using a MAT271 mass spectrometer to determine the content of CH_4 and non-hydrocarbon gases (He, N_2, CO_2, H_2, H_2S). Additionally, a gas chromatograph (Agilent 6890 GC) was employed to analyze hydrocarbon gases such as CH_4, C_2H_6, and C_3H_8. Specifically, the Agilent 6890 GC was equipped with both flame ionization detector (FID) and thermal conductivity detector (TCD), utilizing helium as the carrier gas with a PLOT Al_2O_3 50m-0.53mm capillary column. The gas chromatograph was initially set at 30°C for 10 minutes, followed by a temperature ramp of 10 °C/min up to 180°C, and then held at this temperature for 10 minutes. Both the MAT271 and GC simultaneously measured CH_4 concentrations, allowing for the correction and final experimental results of both non-hydrocarbons and hydrocarbons to be determined.

Using the specialized Noblesse rare gas mass spectrometry system (Nu Instruments), noble gas content and isotope composition were measured (He, Ne, and Ar). The noble gas composition and isotope analysis system includes purification and enrichment systems, a quadrupole mass spectrometer, and a noble gas isotope mass spectrometer. The concentrations of various noble gas components were determined using a quadrupole mass spectrometer (QMG422 PrismaPlus™, Pfeiffer Vacuum), while the isotope ratios were analyzed using the Noblesse rare gas isotope mass spectrometer. Firstly, the sample is purified and separated using a specially designed rare gas preparation line, utilizing cryopumps, activated charcoal, and liquid nitrogen. Subsequently, He, Ne, and Ar are sequentially introduced into the Noblesse mass spectrometer, and their isotope

174   compositions are determined using the peak height ratio method based on ion current signal intensity.

175   The testing procedure is detailed in Cao et al. (2018).

4 Results and discussion

4.1 Geochemical characteristics

4.1.1 Major gas composition

179   The major gas compositions of 14 well samples from the Hetianhe gas field are shown in Table

180   1. The chemical composition of natural gas in the Hetianhe gas field is primarily alkane gases, with

181   small amounts of non-hydrocarbon gases, such as CO_2, N_2, and H_2. The methane (CH_4) content

182   ranges from 72.1% to 85.0%, with an average of 80.0% (Fig. 3a). The heavier hydrocarbons, ethane

183   (C_2) and propane (C_3), collectively account for less than 3% of the total volume. The non-

184   hydrocarbon CO_2 content varies from 0.1% to 15.2%, with an average of 4.1% (Fig. 3b). The N_2

185   content ranges from 7.7% to 18.8%, with an average of 12.9% (Fig. 3c). The gas dryness coefficient

186   (C_1/C_{1-5}) serves as an indicator of hydrocarbon maturity, as long-chain hydrocarbons tend to break

187   into short-chain molecules at higher temperatures or over longer periods of time (Behar et al., 1997;

188   Lorant et al., 1998). The dryness of the gas in the Hetianhe gas field ranges from 0.965 to 0.990

189   (Fig. 3d), indicating that the study area has reached a high-over-maturity stage.
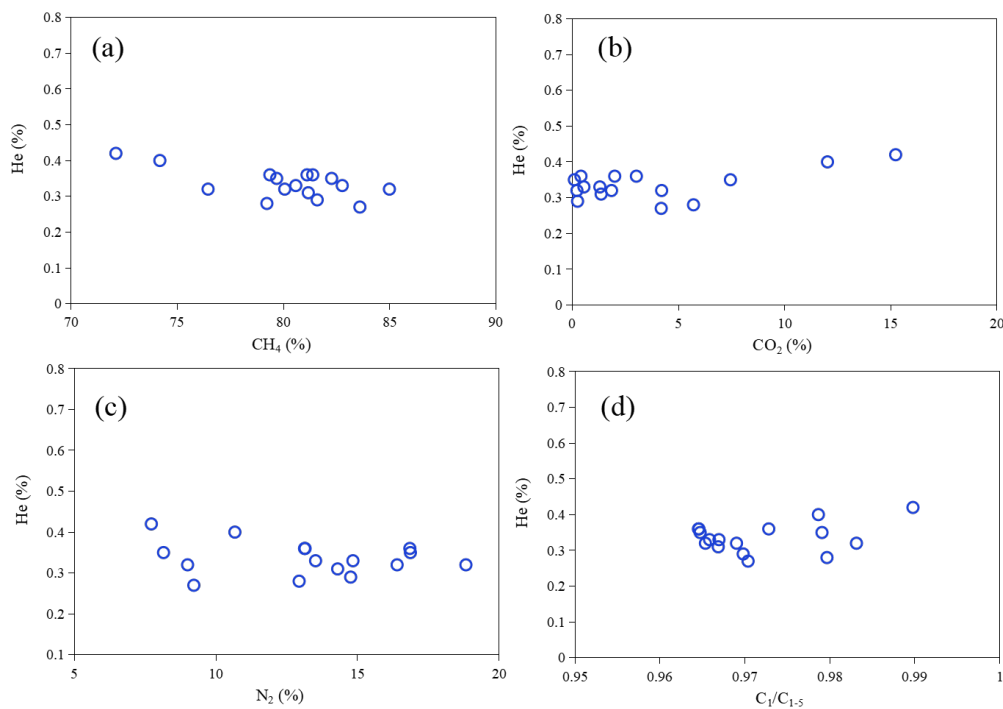
190

191   Fig. 3. Major gas composition characteristics of natural gas in the Hetianhe gas field

192

Table 1. Major gas composition and temperature and pressure conditions of natural gas wells in Hetianhe gas field

| Well | Depth (m) | Formation | Temperature (°C) | Pressure (Mpa) | Gas compositions (%) | | | | | | | | C_1/C_{1-5} |
					CH_4	C_2H_6	C_3H_8	He	N_2	CO_2	H_2	H_2S	
Ma8	1637.00	O	48.0	18.0	72.11	0.34	0.12	0.42	7.72	15.23	0.02	3.54	0.990
Ma3-1H	1596.00	C	53.0	14.8	74.18	0.73	0.31	0.40	10.67	12.02	0.03	0.99	0.979
Ma2	1462.00	C	53.2	15.9	84.99	0.86	0.27	0.32	9.00	4.21	0.02	0.00	0.983
Ma2-1H	1950.00	O	62.0	18.6	82.27	0.96	0.35	0.35	8.15	7.45	0.08	0.00	0.979
Ma5	1960.00	C	62.0	23.8	79.22	0.97	0.34	0.28	12.94	5.71	0.02	0.11	0.980
Ma5-2H	2326.00	O	64.0	22.4	81.11	1.26	0.46	0.36	13.15	3.02	0.01	0.00	0.973
Ma5-4H	2459.00	O	71.0	22.9	83.60	1.15	0.45	0.27	9.22	4.19	0.16	0.00	0.970
Ma4-H1	1931.00	C	58.0	20.4	82.77	1.45	0.62	0.33	13.52	0.55	0.00	0.00	0.967
Ma4-B2H	2116.73	O	69.3	22.4	80.58	1.57	0.62	0.33	14.84	1.30	0.02	0.00	0.966
Ma4-7H	2600.00	C	64.0	20.8	79.68	1.50	0.68	0.35	16.87	0.10	0.00	0.00	0.965
Ma4-H2	2283.00	O	65.0	21.6	81.17	1.53	0.60	0.31	14.30	1.36	0.00	0.00	0.967
Ma4-H6	2782.00	O	71.8	23.0	81.59	1.46	0.55	0.29	14.76	0.25	0.49	0.00	0.970
Ma4-8H	2274.27	O	64.0	22.7	80.06	1.49	0.64	0.32	16.40	0.22	0.04	0.00	0.965
Ma4-12H	2130.00	O	71.1	18.0	76.45	1.36	0.52	0.32	18.83	1.85	0.02	0.00	0.969

193

194

195

196	Table 2. Noble gas abundance and isotopic composition in natural gas samples from the Hetianhe gas field [a].								
Well	^{4}He($\times 10^{-4}$)	^{20}Ne($\times 10^{-7}$)	^{36}Ar($\times 10^{-7}$)	^{3}He/^{4}He (R/Ra)	^{20}Ne/^{22}Ne	^{21}Ne/^{22}Ne	^{40}Ar/^{36}Ar	^{38}Ar/^{36}Ar	V_g/V_w
	cm^3 STP / cm^3 [c]								
Ma3-1H	40±0.2	7.63±0.07	3.18±0.07	0.0536±0.001	9.2±0.23	0.043±0.002	2798±35	0.183±0.002	0.157
Ma2-1H	35±0.2	3.86±0.03	3.17±0.02	0.0611±0.001	9.4±0.21	0.030±0.001	2460±32	0.188±0.001	0.349
Ma5-2H	36±0.1	1.54±0.01	3.21±0.03	0.0532±0.002	9.0±0.21	0.045±0.001	2402±24	0.186±0.002	0.937
Ma4-B2H	33±0.1	0.89±0.01	3.48±0.02	0.0522±0.001	9.0±0.22	0.045±0.003	2181±16	0.182±0.002	1.641
Ma4-7H	35±0.1	1.07±0.05	3.71±0.15	0.0595±0.002	9.3±0.21	0.044±0.001	2129±21	0.182±0.003	1.357
Ma4-H2	31±0.2	0.79±0.01	3.56±0.03	0.0452±0.001	9.1±0.22	0.044±0.001	2050±9	0.177±0.001	1.853
Ma4-12H	32±0.1	1.02±0.02	3.58±0.02	0.0757±0.001	9±0.22	0.045±0.001	2290±26	0.184±0.002	1.434
Air [b]	0.0524	164.5	314.2	1	9.8	0.029	298.56	0.1885	nd [d]

197 Note:

198 [a] 1σ errors are shown in the table after the plus and minus signs.

199 [b] ^{3}He/^{4}He ratios (R) are normalized to air value Ra = 1.4×10^{-6} (Ozima and Podosek, 2002).

200 [c] Noble gas concentrations are in unit of cm^3 STP/cm^3 with standard conditions after Ozima and Podosek, (2002) (p = 0.101 MPa, T = 0 ℃).

201 [d] "nd" denotes no data.

4.1.2 Noble gases

The noble gas concentrations and isotopic compositions are presented in Table 2. Compared to the characteristic values of noble gas concentrations and isotopic ratios in air, the $^4He/^{20}Ne$, $^{21}Ne/^{22}Ne$, and $^{40}Ar/^{36}Ar$ ratios in the samples are significantly higher than the standard atmospheric values, indicating a strong radiogenic crustal origin. Furthermore, except for helium, the concentrations of other noble gases in the samples are substantially lower than the standard atmospheric values, suggesting minimal atmospheric influence and confirming that the samples are not affected by air contamination.

The ^4He concentration in the samples ranges from 0.0031 to 0.004 cm^3 STP/cm^3. The $^3He/^4He$ ratio (R) normalized to the atmospheric $^3He/^4He$ ratio (Ra=1.4×10^{-6}, Ozima and Podosek, 2002) for the samples ranges between 0.045 and 0.076. There is no significant correlation observed between ^4He concentration and $^3He/^4He$ (Fig. 4a). The low $^3He/^4He$ ratio in samples from the Hetianhe gas field indicates a typical crustal origin of helium, with most helium derived from crustal radioactive decay. The typical crustal value for R/Ra is 0.02 (Ballentine and Burnard, 2002).

The ^{20}Ne concentration in the samples ranges from 0.79 to 7.63×10^{-7} cm^3 STP/cm^3. There is a good linear relationship between ^{20}Ne concentration and ^4He concentration (R^2=0.74), indicating that both gases share similar subsurface migration processes. This suggests that before being extracted by natural gas, both were dissolved in formation water and migrated with the water (Fig. 4b). The $^{20}Ne/^{22}Ne$ ratios range from 9 to 9.4, slightly lower than the atmospheric value of 9.8. The $^{21}Ne/^{22}Ne$ ratios range from 0.03 to 0.045, slightly higher than the atmospheric value of 0.029. The neon isotope composition indicates an excess of nucleogenic ^{21}Ne isotope. This trend follows the empirically derived crustal neon production line (Kennedy et al, 1990), suggesting a binary mixing process between atmospheric and crustal endmembers in the gas reservoir (Fig. 4c).

The ^{36}Ar concentrations in the samples range from 3.17 to 3.71×10^{-7} cm^3 STP/cm^3. The measured $^{40}Ar/^{36}Ar$ ratios range from 2050 to 2798, which is significantly higher than the atmospheric ratio of 298.56 (Lee et al., 2006). Due to the $^3He/^4He$ ratio indicating minimal mantle contribution, the excess ^{40}Ar is likely produced by the radioactive decay of potassium in the crust (Fig. 4d).

In summary, the He in the Hetianhe gas field samples is typically crust-derived, while Ne and Ar are considered to be a mixture of atmospheric and crustal components. Over time, radioactive isotopes accumulate from their parent isotopes, with ^{21}Ne produced by nucleogenic reactions from ^{18}O and ^{24}Mg, and ^{40}Ar produced by the β$^+$ decay of ^{40}K. Therefore, atmospheric noble gas isotopes can be used as a normalization standard to calculate the radiogenic components of ^{21}Ne and ^{40}Ar in the samples (Ballentine, 1991).

$$^{21}Ne^* = {}^{21}Ne_{measured} \times (1 - ({}^{21}Ne/^{22}Ne)_{air} / ({}^{21}Ne/^{22}Ne)_{measured}) \tag{1}$$

$$^{40}Ar^*={}^{40}Ar_{measured} \times (1 - ({}^{40}Ar/{}^{36}Ar)_{air} / ({}^{40}Ar/{}^{36}Ar)_{measured})$$ (2)

Where the values of $({}^{21}Ne/{}^{22}Ne)_{air}= 0.029$ and $({}^{40}Ar/{}^{36}Ar)_{air}= 298.56$ (Ozima and Podosek, 2002). The radiogenic components of ^{21}Ne and ^{40}Ar are represented as $^{21}Ne^*$ and $^{40}Ar^*$, respectively.
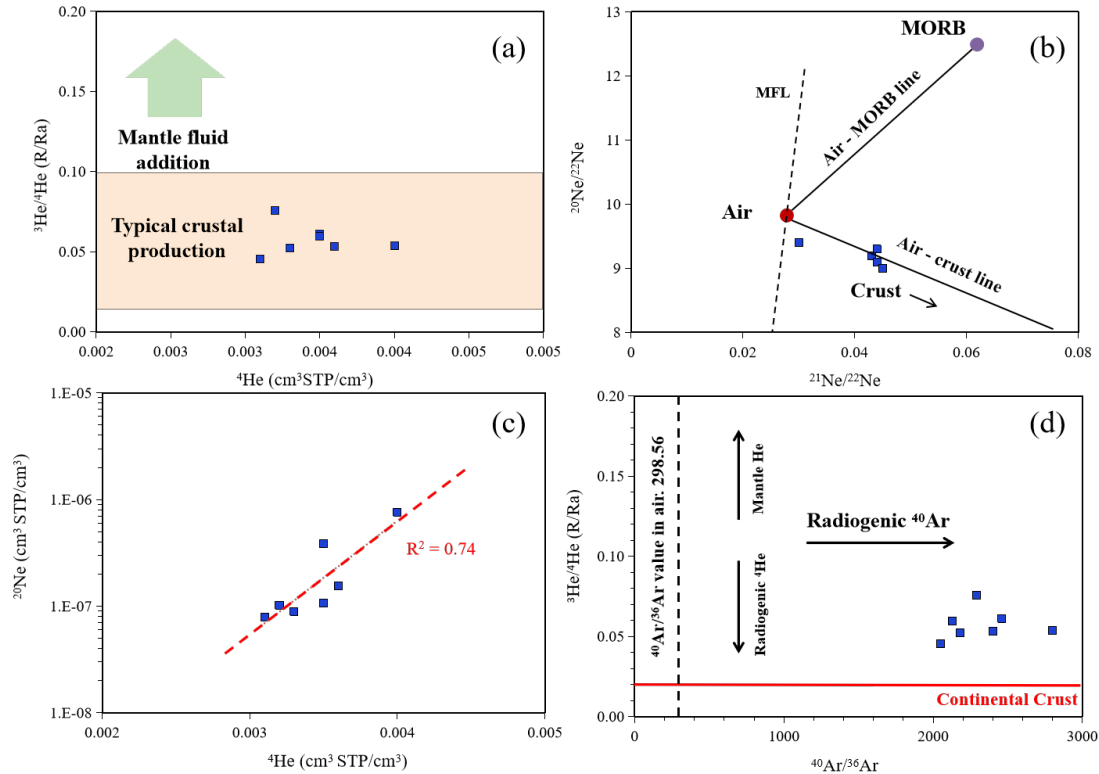
Fig. 4. (a) Relationship between ^4He concentration and helium isotope ratio (R/Ra) of the gas samples. The typical crustal $^3He/^4He$ is about 0.02 (Ballentine and Burnard, 2002). Ratios exceeding 0.1 might be attributed to mantle fluid content, as the $^3He/^4He$ of mid-ocean ridge basalt is usually taken as 8.0 (Dunai and Porcelli, 2002). (b) $^{20}Ne/^{22}Ne$ vs. $^{21}Ne/^{22}Ne$ ratios for all samples in the Hetianhe gas field. Neon ratios in all samples indicate a two-component mixing process between air and crust endmembers. (c) Plot of ^{20}Ne vs. ^4He in the Hetianhe field, showing ^{20}Ne and ^4He have experienced similar subsurface migration processes. (d)$^{40}Ar/^{36}Ar$ ratios vs. R/Ra. $^{40}Ar/^{36}Ar$ ratios in all samples are significantly higher than the air value of 298.56 (Lee et al., 2006).

4.2 Helium distribution pattern

The helium content in Hetianhe gas field ranges between 0.27% and 0.42%, with an average of 0.33%. Hetianhe gas field is located on the Mazatag fault zone, with development from east to west including the eastern production area (Ma4, Ma5 wells), middle production area (Ma2 well), and western production area (Ma3, Ma8 wells). There are significant differences in helium content among different production areas. The average helium content in the eastern production area, middle production area, and western production area is 0.32%, 0.34%, and 0.41% respectively, showing an increasing trend from east to west (Fig. 5). Additionally, helium content shows a negative correlation

with depth, indicating that helium tends to accumulate at higher structural positions as depth decreases (Fig. 6c). There is a weak negative correlation between helium and CH_4 content (Fig. 3a), suggesting that excessive hydrocarbon gases in helium-bearing natural gas reservoirs have a dilution effect on helium (Wang et al., 2020).

Vertically, the helium-bearing reservoirs in Hetianhe gas field are located in the Ordovician and Carboniferous formations, which are thin and adjacent to each other. The helium content in the Carboniferous formation (averaging 0.34%) is slightly higher than that in the lower Ordovician formation (averaging 0.33%), indicating that there is no significant difference in helium content within vertically continuous strata. Previous studies have found that in crustal-source helium reservoirs, the helium content is closely related to reservoir age. The older the reservoir age, the more helium accumulated from radiogenic sources, which is more conducive to receiving helium from deeper sources (Wang et al., 2020; Qin et al., 2022). However, this vertical distribution pattern of helium does not apply in the Hetianhe field, indicating that the accumulation effect of crustal helium over time is not significant. The distribution pattern of helium is complex and controlled by multiple factors.
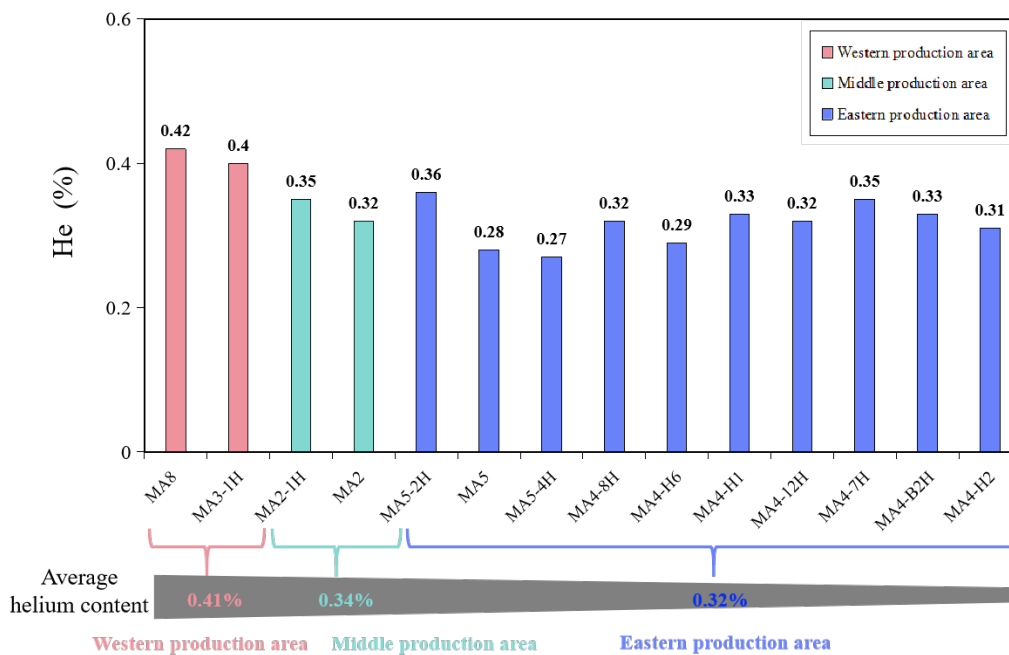
Fig. 5. The helium distribution characteristics in different production areas of the Hetianhe gas field. This indicates that the helium content varies with geographical location from east to west, with higher helium content observed in the western area compared to the eastern area. In addition, helium tends to accumulate in structurally high positions.

4.3 Controlling mechanism on helium accumulation

4.3.1 Temperature and pressure condition

Helium migration and accumulation exhibit characteristics of cross-strata, multi-mechanism processes, and complexity (Brown, 2010; Wang et al., 2023; Cheng et al., 2023; Liu et al., 2024). Helium, as a trace noble gas, does not have a primary generation phase and thus cannot form free gas independently. Its effective migration depends on the carrier role of underground fluids. Previous studies on the mechanism of helium enrichment often emphasize the role of external fluids (such as CH_4, N_2) as "helium pumps", extracting dissolved helium from rock pores (Brown, 2019; Qin et al., 2022; Danabalan et al., 2022; Liu et al., 2023). However, they have insufficiently considered the influence of in-situ changes in temperature and pressure conditions on helium enrichment. In Hetianhe gas field, as the burial depth decreases, the temperature and pressure of the reservoir environment decrease, leading to a significant increase in helium content (Fig. 6). This indicates that the solubility of helium in formation water decreases with decreasing pressure and temperature of the reservoir, causing helium to undergo desolvation during upward migration of helium-bearing fluids. To explore the desolvation process due to changes in temperature and pressure conditions, the desolvation model of helium in rock pore water clearly demonstrates that the solubility of helium in formation conditions is extremely low, primarily controlled by the ambient temperature and pressure conditions (Fig. 7). Compared to the "competitive dissolution" of helium with other gases, changes in ambient temperature and pressure conditions (especially those induced by structural uplift) can lead to continuous desolvation of helium from formation fluids, thereby causing helium enrichment in gas phase. This is consistent with the relative enrichment of helium in higher structural positions in the Hetianhe gas field, where helium content decreases with increasing reservoir depth.

To quantitatively characterize the contribution of uplift-induced desolvation to helium enrichment in the Hetianhe gas field, we calculated the amount of helium desolvation from primary pore water before and after the tectonic uplift during the Himalayan period. We then determined the contribution ratio of helium desolvation during uplift to the current helium reserves in the gas reservoir. According to the burial history of Hetianhe formation (Wang et al., 2007), it is determined that the maximum buried depth of the reservoir before the tectonic uplift in the mountainous period is 2500m, and the current temperature and pressure of the gas reservoir are shown in Table 1. As shown in Table 4, helium desolvation occurred in the in-situ pore water of Hetianhe gas field during the Himalayan tectonic uplift. Due to the difference of tectonic uplift in different production areas, the corresponding amount of helium desolvation is different. The tectonic uplift in the western production area is the largest, and the corresponding helium desolvation amount is also larger. However, it is worth noting that not all wells have de-solubilization. No helium de-solubilization

occurred in Ma4-7H and Ma4-H6 wells in the eastern production area, indicating that the structural uplift in the eastern production area is not obvious. In addition, the contribution of in situ pore water helium desolation caused by tectonic uplift to present gas reservoir helium reserves is 0.029%-0.127%, indicating that the contribution of desolation to helium enrichment is small.

Table 4 Helium exsolution amount in the primary pore water of the Hetianhe gas field before and after the Himalayan tectonic uplift

Well	Depth (m)	W m³ (STP)	Q m³ (STP)	W/Q %
Ma8	1637	3.14E+06	4.14E+09	0.076
Ma3-1H	1596	3.32E+06	3.95E+09	0.084
Ma2	1462	4.01E+06	3.16E+09	0.127
Ma2-1H	1950	2.70E+06	3.45E+09	0.078
Ma5	1960	2.96E+06	2.76E+09	0.107
Ma5-2H	2326	1.28E+06	3.55E+09	0.036
Ma5-4H	2459	7.72E+05	2.66E+09	0.029
Ma4-H1	1931	2.85E+06	3.26E+09	0.087
Ma4-B2H	2116.73	2.20E+06	3.26E+09	0.068
Ma4-7H	2600	-2.08E+04	3.45E+09	/
Ma4-H2	2283	1.57E+06	3.06E+09	0.051
Ma4-H6	2782	-1.13E+06	2.86E+09	/
Ma4-8H	2274.27	1.59E+06	3.16E+09	0.050
Ma4-12H	2130	2.18E+06	3.16E+09	0.069

[a] $W = A H \varphi (1-S_g) C_0 / (1-Z_0) \Delta Z$, where W represents the volume of helium exsolution from in-situ pore water under STP conditions; A is the area of the gas reservoir (m²); H is the average effective thickness of the reservoir (m); φ denotes the average effective porosity of the reservoir (%); S_g is the average gas saturation (%); C_0 is the helium solubility at the original gas reservoir state at a maximum burial depth of 2500 m; ΔZ represents the proportion of helium desorption (%), $\Delta Z = Z_c - Z_0$, where Z is the proportion of free helium in the helium desolation model, and 0 and c respectively represent the maximum burial depth of the reservoir and the current depth; $Z = -3E\text{-}6h^2 + 0.006h + 90.742$ (Zhao et al., 2023).

[b] $Q = A H \varphi S_g B_{ji}$ (Halford et al., 2022), where Q represents the current helium reserves of the gas reservoir under STP conditions; B_{ji} is the initial gas volume factor (Mireault and Dean, 2007), where $B_{ji} = (T_s P_i) / (P_s T_f Z_i)$, where T_s is the base temperature in standard conditions (Rankine), P_i is the initial reservoir pressure in psia [kPa], P_s is the base pressure in standard condition (14.65 psia

[101.35 kPa]), T_f is the formation temperature in Rankine, and Z_i is the compressibility at reservoir

pressure and temperature of the dominant gas (Peng and Robinson, 1976).
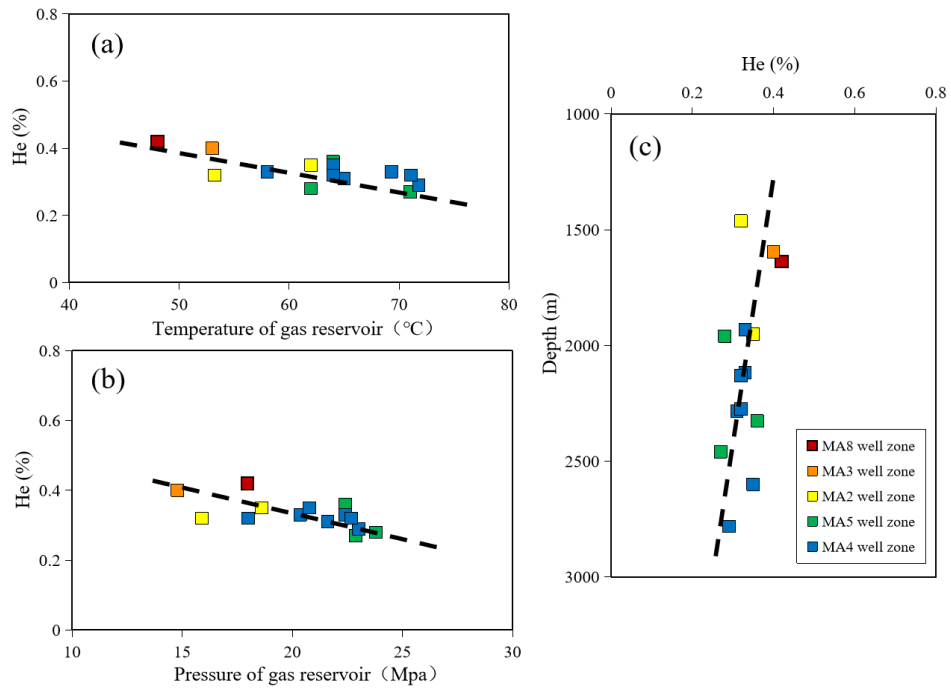
Fig. 6. Relationship between helium content, gas reservoir depth, temperature and pressure

conditions in the Hetianhe gas field
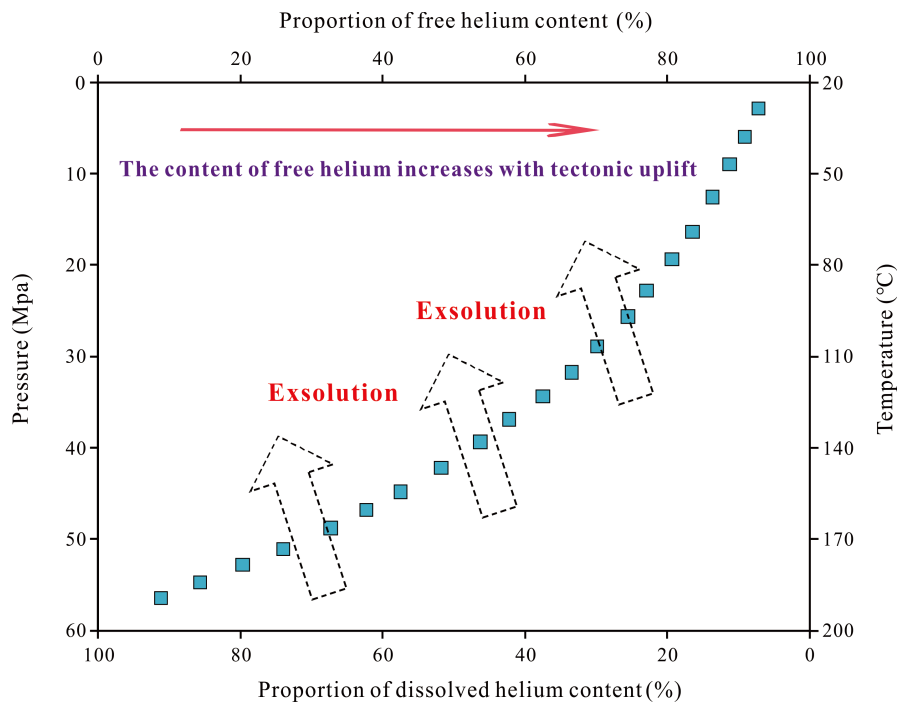
Fig. 7. He desolation model in rock pore water (Modified from Zhao et al., 2023); Simulation

conditions: surface temperature 20 ℃, formation temperature gradient 30℃ /km, formation

pressure gradient 10 MPa/km. Under these conditions, the proportion of free He occurring in a

342   unit volume of granite (decay time 400 Ma, χ_{He}=5%) with various temperature and pressure is

343   simulated.

4.3.2 Lateral migration

345   Most helium-rich gas fields typically develop in shallow depths (less than 2 km), where deep-

346   seated helium fluid migration plays a crucial role in helium enrichment. Noble gases are widely

347   used to trace underground fluid migration and interactions. Air-derived noble gases (ANG), such as:

348   ^{20}Ne, ^{36}Ar, ^{84}Kr, ^{130}Xe) are initially introduced from air saturated water (ASW) and can be used to

349   constrain hydrocarbon or aqueous phase interactions and histories (Ballentine and Burnard, 2002;

350   Zhou et al., 2005; Barry et al., 2016; Barry et al., 2017; Zhang et al., 2019; Halford et al., 2022).

351   ASW has a distinct composition of atmospheric noble gases (Kipfer et al., 2002). When natural gas

352   interacts with groundwater, due to different solubilities, ANG preferentially partition into the gas

353   phase. In this framework, assuming ASW infiltrates into the underground fluid system via

354   groundwater recharge, a gas-phase solubility model can be used to reconstruct the volume of

355   groundwater encountered during the interaction between a given gas phase and subsurface fluids.

356   The gas-water volume ratio (V_g/V_w) indicator is employed to quantify the pathway of subsurface

357   helium-bearing fluid migration. The V_g/V_w can be calculated according to Ballentine et al. (2002).

$$\frac{V_g}{V_w} = \frac{\rho_w C_i^{asw}}{C_i^{sample}} - \frac{16 T \rho_w}{195 \gamma_i K_i^m} \tag{3}$$

359   Where ρ_w is the density of water; T is the reservoir temperature; γ_i is the Setschenow coefficient

360   which accounts for non-ideality resulting from salinity; C_i^{sample} and C_i^{asw} are the concentrations with

361   units of cm^3 STP / cm^3 in the sample and ASW respectively; and K_i^m is the Henry's law constant

362   with unit of atm Kg/mol.

363   The V_g/V_w of the sample in this study was calculated using the air-derived noble gas ^{20}Ne, and

364   the corresponding calculated V_g/V_w results are shown in Table 2. The variation of V_g/V_w across

365   different production areas in the Hetianhe gas field is significant. Moving from the eastern

366   production area to the central and western production areas, V_g/V_w decreases gradually (1.40, 0.35,

367   0.16), while the helium content in natural gas increases progressively (0.32%, 0.34%, 0.41%). This

368   east-west difference in V_g/V_w in the Hetianhe field suggests that a greater gas phase migration

369   distance is required from east to west to facilitate more interaction between the given gas phase and

370   groundwater supplying ^{20}Ne. In addition, V_g/V_w shows a negative correlation with ^{4}He (Fig. 8a),

371   while ^{4}He correlates positively with ^{21}Ne* and ^{40}Ar* (Fig. 8b, c). This indicates that low V_g/V_w is

372   closely associated with higher concentrations of radioactive rare gases. During underground natural

373   gas migration, more radioactive isotopes from the crust are continuously extracted. Similar

374   phenomena have been observed in gas fields in southwestern Tanzania and the Haynesville shale

375   play in the United States (Byrne et al., 2020; Mtili et al., 2021). This further underscores that

376   increased gas phase migration distance is a critical factor in helium enrichment.

377   Therefore, a larger migration distance is the key factor in generating the low V_g/V_w ratios. The

378   V_g/V_w index indicates lateral migration of underground helium-bearing natural gas from east to west

379   in the Hetianhe gas field. As the migration distance increases, helium-bearing natural gas

380   continuously extracts and captures radioactive isotopes during migration. This process represents

381   the primary mechanism for helium enrichment in the Hetianhe gas field.

382
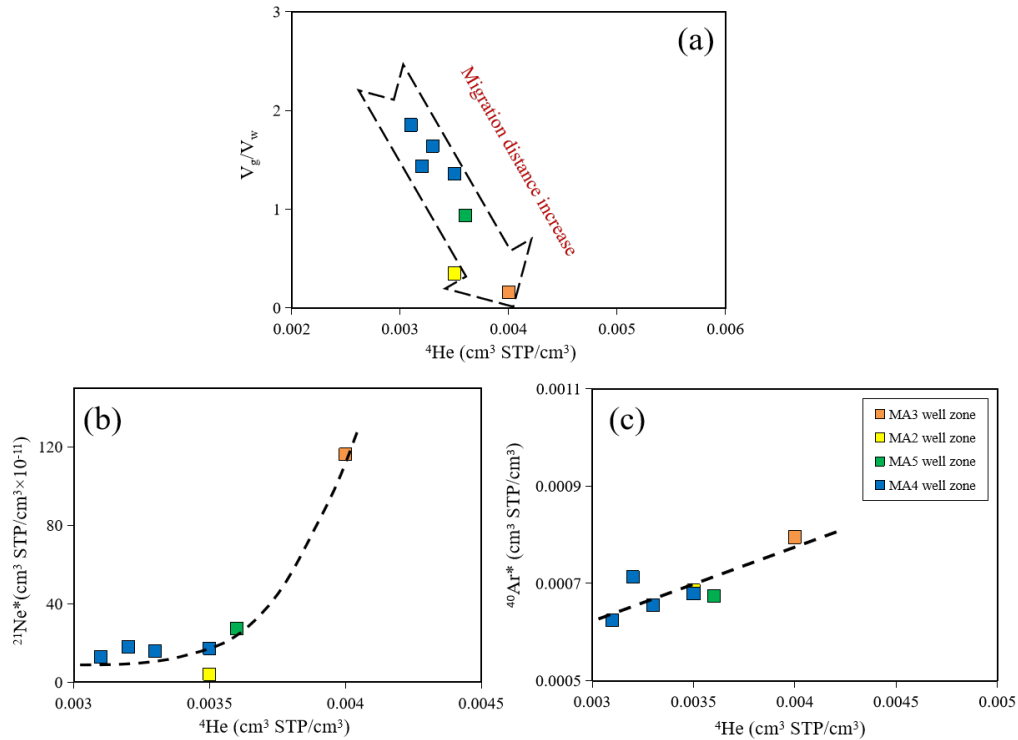
383

384   Fig. 8. (a) V_g/V_w ratio vs. ^{4}He concentration. In this study, the concentration of noble gases in

385   seawater at 10 °C was taken as the initial concentration of noble gases in ASW. (b-c) ^{4}He

386   concentrations correlate with the radiogenic ^{21}Ne* and ^{40}Ar* concentrations. The radiogenic

387   components of ^{21}Ne and ^{40}Ar are represented by ^{21}Ne* and ^{40}Ar*, respectively.

4.3.3 Cap distribution

389   Helium commonly coexists as an associated gas with natural gas. Similar to the formation and

390   storage of natural gas, it is in a dynamic equilibrium of continuous supply and loss. However, due

391   to the dynamic equilibrium of natural gas migration and the characteristics of late-stage

392   accumulation, helium requires more stringent preservation conditions compared to hydrocarbon

393   gases (Wang et al., 2023; Liu et al., 2023; Tao et al., 2024). In particular, helium molecules have a

394   diameter of only 0.26 nm, much smaller than other hydrocarbon and non-hydrocarbon gases (such

395   as CO_2, N_2), which gives them strong diffusion capabilities (Torgersen et al., 1985). In addition,

396   during late-stage intense tectonic activities that disrupt reservoir adjustments, the loss of helium gas

397 is significantly higher than hydrocarbon gases (Chen et al., 2019). Therefore, the accumulation and
398 preservation of helium require effective capping layer and sealing conditions. The paste mudstone,
399 in particular, can serve as an effective barrier against helium diffusion, providing a good sealing
400 effect for containing helium gas. Tyne et al. (2022) used numerical simulation to establish a diffusion
401 release model for helium in the Greater Aneth oil field and Lisbon Southeast gas field in the Paradox
402 Basin. They found that the gypsum mudstone of the Pennsylvanian Paradox Formation acts as
403 effective barriers against vertical gas diffusion within the basin, impeding helium from vertically
404 migrating towards shallower strata (Tyne et al., 2022).

405 The Hetianhe helium-rich gas reservoir mainly exists in the Carboniferous and Ordovician
406 buried hills, and its direct covering layer is the gypsum mudstone of the Bachu and Kalashai
407 formations of the Carboniferous. It can be seen that the cap thickness of Hetianhe gas field is
408 positively correlated with the helium content of the gas reservoir (Fig. 9), and the storage conditions
409 of the cap control the differential distribution of helium. Therefore, the distribution of gypsum and
410 mudstone cap in the east-west direction limits the vertical diffusion of helium, which controls the
411 differential enrichment of helium from a macro perspective.
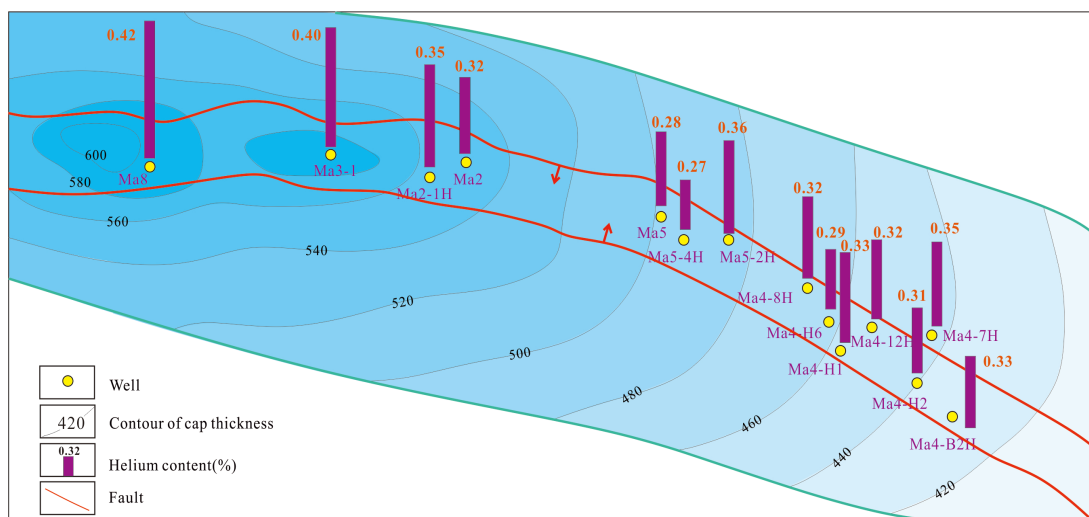
Fig. 9. Distribution of cap thickness and helium content in the Hetianhe gas field

4.4 Helium enrichment model

415 The enrichment of helium in each production area of Hetianhe gas field has similar geological
416 background and geological process. The mechanisms controlling the differential distribution of
417 helium involve reservoir conditions, lateral migration, and preservation conditions. Based on the
418 discussion above, a five-stage conceptual model can be established to explain the differential
419 enrichment of helium in the Hetianhe gas field (Fig. 10):

420 (1) Atmosphere saturated groundwater (ASW) infiltrates into the subsurface fluid system
421   through meteoric water recharge.

(2) Helium generated from the decay of radioactive elements U and Th in the crust is released from rocks and dissolved into pore-fracture water.

(3) During multiple tectonic movements, deep-seated helium migrates towards shallower depths through formation water, leading to widespread distribution of dissolved helium in sedimentary formations. During the migration of dissolved helium in formation water, changes in temperature and pressure can cause minor helium desolvation.

(4) During the Himalayan period, hydrocarbon source rocks undergo episodic hydrocarbon expulsion, and natural gas migrates from deeper layers to traps through migration pathways. During this migration, interaction with formation water in pores and fractures causes extraction, and degassing from groundwater into the gas phase, where it accumulates together with the carrier natural gas in reservoirs.

(5) When natural gas migrates laterally in reservoirs, it continuously extracts helium from formation water. As the migration distance increases, more helium is captured. In the Hetianhe gas field, from the eastern production area to the western production area, the V_g/V_w ratio decreases gradually (1.40, 0.35, 0.16), while the helium content in natural gas increases progressively (0.32%, 0.34%, 0.41%).
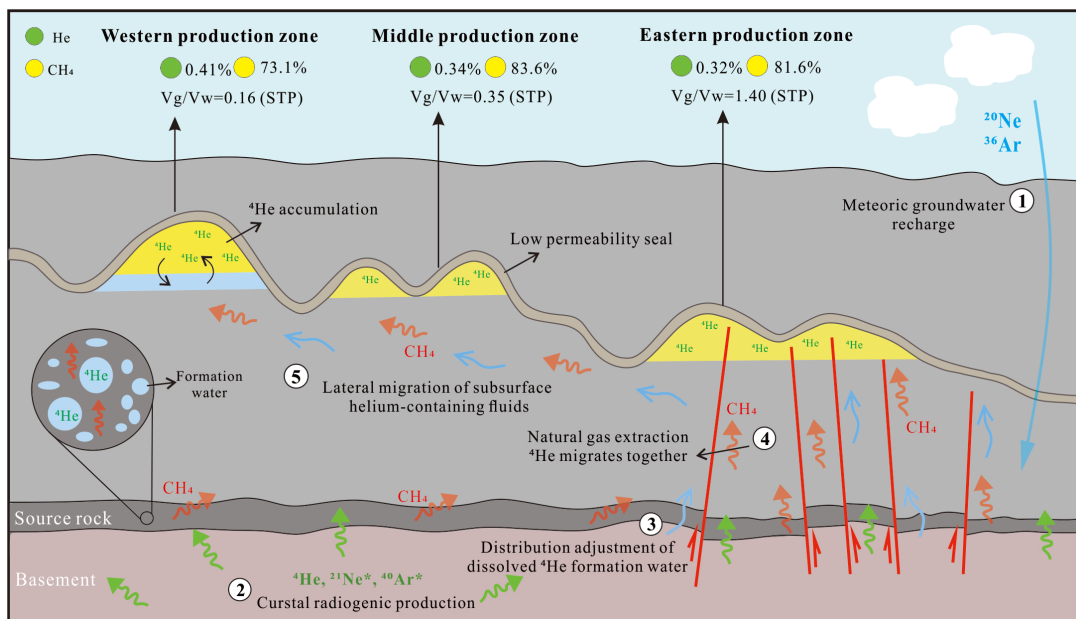
Fig. 10. Helium differential enrichment model of Hetianhe gas field. Groundwater is commonly ubiquitous underground and is often replenished by meteoric water, characterized by air-saturated water (ASW). Decay of radioactive crustal elements occurs throughout the crust and release helium, which dissolves into pore and fracture waters. Through later tectonic adjustments, the distribution of dissolved helium in formation water is dispersed across sedimentary formations. The phase equilibrium between groundwater and hydrocarbon fluids is rapid on geological time

446   scales, and this represents the primary pathway for ^{4}He enrichment in hydrocarbon fluids.

5 Conclusions

448   This study reports on natural gas composition and noble gas isotope data from three production
449 areas in the Hetianhe gas field, Tarim Basin. It investigates the mechanism of helium enrichment in
450 this helium-rich gas field. A model has been established to reveal the controlling mechanisms of
451 helium differential enrichment. The helium content in the Hetianhe gas field ranges from 0.27% to
452 0.42%, with an average of 0.33%, indicating it is a helium-rich natural gas reservoir. Helium content
453 increases gradually from east to west on a planar scale, and helium tends to enrich in structurally
454 higher positions. Vertically, there is no significant difference in helium content within vertically
455 continuous strata. The samples' ^{3}He/^{4}He ratios range from 0.045 to 0.076 Ra, with an average of
456 0.057 Ra, indicating that helium is predominantly crust-derived (99%).

457   Helium migration and accumulation exhibit characteristics of cross-stratal movement, multiple
458 mechanisms, and complexity. The controlling mechanisms of helium differential enrichment mainly
459 manifest in temperature-pressure conditions, lateral migration, and preservation conditions.
460 Changes in temperature and pressure, especially differences caused by tectonic uplift, lead to
461 degassing, resulting in relative enrichment of helium in structurally high positions. A gas solubility
462 model was used to identify the subsurface fluid migration pathways. It is found that from the eastern
463 production area to the middle production area and then to the western production area, the V_g/V_w
464 ratio gradually decreases, corresponding 1.40, 0.35, 0.16, respectively. The V_g/V_w ratio index
465 indicates that helium-rich natural gas undergoes lateral migration from east to west, and as the
466 migration distance increases, the content of radioactive isotopes gradually increases. This suggests
467 that during the migration, the helium-rich natural gas continuously extracts radiogenic isotopes,
468 leading to the differential enrichment of helium. It is noteworthy that, compared to degassing, the
469 extraction process may be the primary mechanism for helium enrichment in the Hetianhe gas field.
470 Additionally, the distribution of east-west gypsum-mudstone cap layers results in differential
471 vertical diffusion of helium, which macroscopically controls the differential enrichment of helium.
472 The migration and accumulation of helium exhibit a certain synergy with hydrocarbon reservoir
473 formation. Ultimately, a five-stage conceptual model has been developed to explain the differential
474 enrichment of helium in the Hetianhe gas field: (1) Groundwater recharge; (2) Generation and
475 release of helium; (3) Adjustment of dissolved helium distribution in formation water; (4) Extraction
476 of helium by natural gas migration and accumulation; (5) Lateral migration leading to differential
477 distribution of helium.

References

Ballentine C. J. and Burnard P. G. 2002. Production, release and transport of noble gases in the continental crust. Rev. Mineral. Geochem. 47, 481–538.

Ballentine, C.J., Burgess, R., Marty, B. 2002. Tracing fluid origin, transport and interaction in the crust. Rev. Mineral. Geochem. 47, 539-614.

Ballentine, C.J., O'Nions, R.K., Oxburgh, E.R., Horvath, F., Deak, J. 1991. Rare gas constraints on hydrocarbon accumulation, crustal degassing and groundwater flow in the Pannonian Basin. Earth Planet Sci. Lett. 105, 229–246.

Ballentine, C.J., Sherwood Lollar, B. 2002. Regional groundwater focusing of nitrogen and noble gases into the Hugoton-Panhandle giant gas field, USA. Geochem. Cosmochim. Acta. 66, 2483–2497.

Barry, P.H., Lawson, M., Meurer, D. Danabalan, Mabry, J.C., Ballentine, C.J. 2017. Determining fluid migration and isolation times in multiphase crustal domains using noble gases. Geology 45 (9), 775–778.

Barry, P.H., Lawson, M., Meurer, W.P., Warr, O., Mabry, J.C., Byrne, D.J., Ballentine, C. J. 2016. Noble gases solubility models of hydrocarbon charge mechanism in the Sleipner Vest gas field. Geochim. Cosmochim. Acta 194, 291–309.

Behar, F., Vandenbroucke, M., Tang, Y., Marquis, F., Espitalie, J. 1997. Thermal cracking of kerogen in open and closed systems: determination of kinetic parameters and stoichiometric coefficients for oil and gas generation. Org. Geochem. 26 (5), 321-339.

Brown, A., 2010. Formation of High Helium Gases: a Guide for Explorationists 2010, AAPG Conference. New Orleans, Louisiana, USA, 11-14.

Brown, A., 2019. Origin of helium and nitrogen in the Panhandle–Hugoton field of Texas, Oklahoma, and Kansas, United States. AAPG Bull. 103, 369-403.

506 Byrne, D.J., Barry, P.H., Lawson, M., Ballentine, C.J. 2020. The use of noble gas isotopes to

507 constrain subsurface fluid flow and hydrocarbon migration in the East Texas Basin. Geochim.

508 Cosmochim. Acta 268, 186–208.

509 Cai, C., Worden, R.H., Wang, Q., Xiang, T., Zhu, J., & Chu, X. 2002. Chemical and isotopic

510 evidence for secondary alteration of natural gases in the Hetianhe Field, Bachu Uplift of the

511 Tarim Basin. Organic Geochemistry, 33, 1415-1427.

512 Cao, C., Zhang, M., Tang, Q., Yang, Y., Lv, Z., & Zhang, T. 2018. Noble gas isotopic variations and

513 geological implication of longmaxi shale gas in sichuan basin, china. Mar. Petrol. Geol. 89(10),

514 38-46.

515 Chen, B., Stuart, F.M., Xu, S., Györe, D., & Liu, C. 2019. Evolution of coal-bed methane in

516 Southeast Qinshui Basin, China: Insights from stable and noble gas isotopes. Chemical

517 Geology, 529, 119298.

518 Chen, J.F., Xu, Y.C., Huang, D.F., 2000. Geochemical characteristics and origin of natural gas in

519 Tarim Basin, China. AAPG (Am. Assoc. Pet. Geol.) Bull. 84 (5), 591–606.

520 Cheng, A., Sherwood Lollar, B., Gluyas, J.G., & Ballentine, C.J. 2023. Primary N_2–He gas field

521 formation in intracratonic sedimentary basins. Nature, 615, 94-99.

522 Dai, J., Ni, Y., Qin, S., Huang, S., Gong, D., Liu, D., Feng, Z., Peng, W., Han, W., Fang, C., 2017.

523 Geochemical characteristics of He and CO2 from the Ordos (cratonic) and Bohaibay (rift)

524 basins in China. Chem. Geol. 469, 192-213.

525 Danabalan, D., Gluyas, J., Macpherson, C., Abraham-James, T., Bluett, J., Barry, P., Ballentine, C.J.,

526 2022. The Principles of Helium Exploration. Petroleum Geoscience. 28 (2).

527 Du, Y., Fan, T., Machel, H.G., Gao, Z., 2018. Genesis of Upper Cambrian-Lower Ordovician

528 dolomites in the Tahe Oilfield, Tarim basin, NW China: several limitations from petrology,

529 geochemistry, and fluid inclusions. Mar. Petrol. Geol. 91, 43–70.

530 Dunai T. J. and Porcelli D., 2002. Storage and Transport of Noble Gases in the Subcontinental

531 Lithosphere. Rev. Mineral. Geochem. 47, 371–409.

532 Feng, Z., Hao, F., Hu, L., Hu, G., Zhang, Y., Li, Y., Wang, W., Li, H., Xiao, J., Tian, J., 2024. Source,

533 migration and accumulation of helium under deep hydrothermal fluid activities. Petroleum

534 Exploration and Development, 51(3): 1-12.

535 Guo, Y., Zhao, G., Guo, R., Han, Y., Wei, Z., Zhou, N., & Ju, P., 2022. Late Paleoproterozoic

536   orogenic evolution of the northern Tarim Craton, NW China: Insights from phase equilibrium

537   modeling and zircon U-Pb geochronology of metapelitic granulite in the Kuluketage area.

538   Gondwana Research.

539   Halford, D. T., Karolyt, R., Barry, P. H., Whyte, C. J., Darrah, T. H., & Cuzella, J. J., 2022. High

540   helium reservoirs in the four corners area of the colorado plateau, usa. Chemical Geology, 596,

541   120790.

542   Kennedy B., Hiyagon H. and Reynolds J. 1990 Crustal neon: a striking uniformity. Earth Planet.

543   Sci. Lett. 98, 277–286.

544   Kipfer R., Aeschbach-Hertig W., Peeters F. and Stute M. 2002. Noble gases in lakes and ground

545   waters. Rev. Mineral. Geochem. 47, 615–700.

546   Lai, J., Liu, S.C., Xin, Y., Wang, S., Xiao, C.W., Song, Q.Q., Chen, X., Yang, K.F., Wang, G. W.,

547   Ding, X.J., 2021. Geological-petrophysical insights in the deep Cambrian dolostone reservoirs

548   in Tarim Basin, China. AAPG (Am. Assoc. Pet. Geol.) Bull. 105 (11), 2263–2296.

549   Lee, J.Y., Marti, K., Severinghaus, J.P., Kawamura, K., Yoo, H.S., Lee, J.B., Kim, J.S., 2006. A

550   redetermination of the isotopic abundances of atmospheric Ar. Geochim. Cosmochim. Acta 70

551   (17), 4507–4512.

552   Liu, K., Chen, J., Fu, R., Wang, H., Luo, B., Chen, Z., Dong, Q., Dai, X., Zhang, B., 2023.

553   Distribution characteristics and controlling factors of helium-rich gas reservoirs. Gas Science

554   and Engineering 110, 204885.

555   Liu, Q., Jin, Z., Wang, Y., Li, J., Liu, W.i, Liu, Z. 2009. Genetic type and distribution of natural gas

556   in Tarim Basin. Acta Petrolei Sinica. 30, 46-50.

557   Liu, Q., Li, P., Zhu, D., Zhu, D., Wu, X., Wang, X., Tao, X., Meng, Q., Xu, H., Gao, Y., & Zhou, Z.

558   2024. Helium resource in the petroliferous basins in China and its development prospects. Cell

559   Reports Physical Science, 5, 102031.

560   Lorant, F., Prinzhofer, A., Behar, F., Huc, A.-Y., 1998. Carbon isotopic and molecular constraints on

561   the formation and the expulsion of thermogenic hydrocarbon gases. Chem. Geol. 147 (3), 249-

562   264.

563   Mireault, R., Dean, L., 2007. Reservoir engineering for geologists. Part 3: volumetric estimation.

564   Can. Soc. Petrol. Reservoir Geologists 34, 11–14.

565   Mtili, K.M., Byrne, D., Tyne, R.L., Kazimoto, E., Kimani, C.N., Kasanzu, C.H., Hillegonds, D.J.,

566   Ballentine, C.J., & Barry, P.H. 2021. The origin of high helium concentrations in the gas fields
567   of southwestern Tanzania. Chemical Geology. 585, 120542.

568   Ozima M. and Podosek F. A. 2002. Noble Gas Geochemistry. Cambridge University Press,
569   Cambridge.

570   Peng, D., Robinson, D.B., 1976. A new two-constant equation of state. Ind. Eng. Chem. Fundam.
571   15, 59–64.

572   Qin, S., Xu, D., Li, J., Zhou, Z., 2022. Genetic Types, Distribution Patterns and Enrichment
573   Mechanisms of Helium in China's Petroliferous Basins. Front. Earth Sci. 10, 675109.

574   Qin, S., Zou, C., Dai, J., Li, M., Hu, J., Zhang, Q., Lu, Y. 2006. Water-soluble gas accumulation
575   process of Hetianhe gas field in Tarim Basin,NW China, Petroleum Exploration and
576   Development, 33. (3): 282-288.

577   Ren, Q., Feng, J., Johnston, S.T., & Zhao, L. 2021. The influence of argillaceous content in
578   carbonate rocks on the 3D modeling and characterization of tectonic fracture parameters—
579   example from the carboniferous and ordovician formations in the hetianhe gas field, Tarim
580   Basin, NW China. Journal of Petroleum Science and Engineering, 108668.

581   Siddhantakar, A., Santillán-Saldivar, J., Kippes, T., Sonnemann, G.W., Reller, A., & Young, S.B.
582   2023. Helium resource global supply and demand: Geopolitical supply risk analysis. Resources,
583   Conservation and Recycling. 193, 106935.

584   Song, D., Wang, T., Li, M., Ni, Z. 2015. Source of the condensates from the Hetianhe Field and the
585   genetic relationship between the condensates and their associated gases. Science China: Earth
586   Sciences, 45(07): 941-952 (in Chinese).

587   Tao, S., Yang, Y, Cheng, Y., et al. 2024. Geological conditions, genetic mechanisms, and
588   accumulation patterns of helium resources. Petroleum Exploration and Development, 51(2): 1-
589   17.

590   Tao, X., Li, J.., Zhao, L., Li, L., Zhu, W., Xin, L., Su, F., Shan, X., Zheng, H., Zhang, L., 2019.
591   Helium resources and discovery of first supergiant helium reserve in China: Hetianhe gas field.
592   Earth Sci. 44 (3), 1024–1041.

593   Torgersen, T., Clarke, W. 1985. Helium accumulation in groundwater, I: An evaluation of sources
594   and the continental flux of crustal 4 He in the Great Artesian Basin, Australia. Geochimica et
595   Cosmochimica Acta, 49 (5): 1211-1218.

Tyne, R.L., Barry, P.H., Cheng, A., Hillegonds, D.J., Kim, J., McIntosh, J.C., & Ballentine, C.J. 2022. Basin architecture controls on the chemical evolution and ^{4}He distribution of groundwater in the Paradox Basin. Earth and Planetary Science Letters. 589, 117580.

Wang, X., Liu, Q., Liu, W., Li, X., Tao, C., & Li, X., et al. 2023. Helium accumulation in natural gas systems in chinese sedimentary basins. Marine and Petroleum Geology, 150, 106155.

Wang, X., Liu, W., Li, X., Liu, Q., & Xu, Y. 2020. Radiogenic helium concentration and isotope variations in crustal gas pools from sichuan basin, china. Applied Geochemistry, 117, 104586.

Wang, Z., Wang, Q., Wang, Y., 2000. Reservoir forming conditions and controlling factors in hetian river gas field, Tarim Basin. Marine Origin Petroleum Geology (Z1), 124-132(in Chinese).

Wang, Z., Wang, Q., Zhao, M., Li, Y., Xu, Z. 2007. Geochemical characteristics and accumulation process of natural gas in the Tarim Basin and the Tian He gas field. Sci. China; 37 (Suppl. II): 69-79 (in Chinese).

Wu, G., Zhu, H., Zhang, L., Wang, C., Zhou, B. 2011. Recognition of the Ordovician carbonate reservoir types of the Hetianhe Gas Field,Tarim Basin,and lts Significance. Natural gas industry, 31 (7): 5-10, 101-102(in Chinese).

Zhang, W., Li, Y., Zhao, F., Han, W., Li, Y., Wang, Y., Holland, G., Zhou, Z., 2019a. Using noble gases to trace groundwater evolution and assess helium accumulation in Weihe Basin, central China. Geochim. Cosmochim. Acta 251, 229-246.

Zhang, W., Li, Y., Zhao, F., Han, W., Zhou, J., Holland, G., & Zhou, Z. 2019b. Quantifying the helium and hydrocarbon accumulation processes using noble gases in the North Qaidam Basin, China. Chemical Geology. 525, 368-379.

Zhao, D., Wang, X., Liu, W., Zhang, D., Li, X., Zhang, j. 2023. Calculation method and geological significance of dissolved and exsolved helium in pore water. Natural Gas Industry, 43(2): 155-164.

Zhou, Z., Ballentine, C.J., Kipfer, R., Schoell, M., Thibodeaux, S., 2005. Noble gas tracing of groundwater/coalbed methane interaction in the San Juan Basin, USA. Geochim. Cosmochim. Acta 69 (23), 5413-5428.

Zhu, G., Zhang, Y., Zhou, X., Zhang, Z., Du, D., & Shi, S., et al. 2019. TSR, deep oil cracking and exploration potential in the hetianhe gas field, tarim basin, china. Fuel, 236, 1078-1092.